

Graphene as a tunable THz reservoir for shaping the Mollow triplet of an artificial atom via plasmonic effects

Ebrahim Forati* and George W. Hanson†

Department of Electrical Engineering, University of Wisconsin–Milwaukee, Milwaukee, Wisconsin 53211, USA

Stephen Hughes‡

Department of Physics, Engineering Physics and Astronomy, Queen's University, Kingston, Ontario, Canada K7L3N6

(Received 29 April 2014; revised manuscript received 30 June 2014; published 12 August 2014)

Using a realistic quantum master equation, we show that the resonance fluorescence spectra of a two-level artificial atom (quantum dot) can be tuned by adjusting its photonic local density of states via biasing one or more graphene monolayers. The structured photon reservoir is included using a photon Green function theory which fully accounts for the loss and dispersion. The field-driven Mollow triplet spectrum can be actively controlled by the graphene bias in the THz frequency regime. We also consider the effect of a dielectric support environment and multiple graphene layers on the emitted fluorescence. Finally, thermal bath effects are considered and are shown to be important for low THz frequencies.

DOI: [10.1103/PhysRevB.90.085414](https://doi.org/10.1103/PhysRevB.90.085414)

PACS number(s): 78.67.Wj, 42.50.Pq, 73.20.Mf, 78.67.Bf

I. INTRODUCTION

It is highly desirable to electronically manipulate the photonic spectrum of a multilevel emitter such as an atom or quantum dot (QD). While it is well known that the spectrum is influenced by the photon emitter's electromagnetic environment (e.g., via the Purcell effect [1]), engineering the environment to obtain desirable characteristics often results in a fixed structure that is not actively tunable. Surface plasmon polaritons (SPPs) on graphene [2–5] are highly tunable and offer a promising way to achieve electronic control over an emitter's spectrum through interactions with graphene SPPs. Recent scattering-type scanning near-field optical microscopy (SNOM) imaging experiments [6] have demonstrated in real space the excitation of graphene SPPs on finite graphene structures, and in [7] excitation and damping of SPPs on graphene structures were investigated experimentally for graphene on several substrates. Additionally, graphene quantum plasmonics has been considered in [8], where vacuum Rabi splitting was shown, and in [9], where active control over a quantum state via biasing was demonstrated.

When placed in the vicinity of a multilevel emitter, graphene, along with the vacuum density of electromagnetic field modes, forms the photonic reservoir with which the emitter interacts. The spectral and statistical properties of such a system are strongly dependent on the reservoir mode density via the local density of states (LDOS) [10]. In [11], the reservoir of electromagnetic modes is altered by the presence of a metal nanoparticle, and the resonance fluorescence was examined in the vicinity of the nanoparticle plasmon resonance. Several disadvantages of this system are that the LDOS is not tunable and placing a photon emitter at the desired spatial position is challenging. From a practical viewpoint, one desires a spatial position that is translationally invariant, e.g., near a surface, with an LDOS that can be tuned in a controllable manner.

In this work we use translationally invariant graphene, which is electronically tunable, to alter the reservoir for a two-level artificial atom (hereafter referred to as a QD) in a controllable manner. Furthermore, it is known that a graphene support structure consisting of a dielectric layer can play a role in shaping the LDOS [12], and so we also consider the effect of a substrate on the resonance fluorescence. Since the plasmon response of graphene exhibits a strong dependence on bias in the low to middle THz (meV) frequency regime, we model pump fields and QD excitons at these frequencies [13,14]. After obtaining the LDOS properties of the medium, we derive and solve a quantum master equation to demonstrate control over the Mollow triplet [15,16] of a QD by a nearby graphene sheet. The complex reservoir including the graphene constitutes a lossy inhomogeneous environment for the QD, and here we use a rigorous photon Green function theory applicable to arbitrary lossy media [17]. The Mollow triplet is caused by coherent Rabi oscillations and quantum fluctuations and is of fundamental importance. In addition to exploring how the Mollow triplet changes with a tunable graphene layer, we also show that thermal bath effects are important for low THz frequencies.

II. QUANTUM MASTER EQUATION AND GREEN FUNCTION THEORY

Figure 1 shows the geometry under consideration, consisting of a QD which is a distance d from an infinite graphene sheet. The polarization of the pump field is aligned with the dipole moment, perpendicular to the graphene surface. The Hamiltonian of the coupled system is the sum of the QD, pump, reservoir (graphene plus vacuum), and their interaction,

$$\begin{aligned}
 H_S &= \hbar\omega_x\sigma^+\sigma^-, & H_{\text{pump}} &= \frac{\hbar\Omega}{2}(\sigma^+e^{-i\omega_L t} + \sigma^-e^{+i\omega_L t}), \\
 H_R &= \hbar \int d\mathbf{r} \int_0^\infty \omega \mathbf{f}^\dagger(\mathbf{r},\omega) \mathbf{f}(\mathbf{r},\omega) d\omega, & & (1) \\
 H_I &= - \left[\sigma^+ \int_0^\infty \mathbf{d} \cdot \mathbf{E}(\mathbf{r}_d,\omega) d\omega + \text{H.c.} \right], & &
 \end{aligned}$$

*eforati@uwm.edu

†george@uwm.edu

‡shughes@physics.queensu.ca

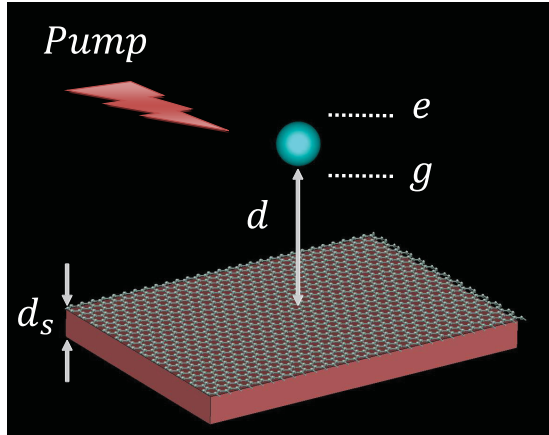


FIG. 1. (Color online) Schematic of a driven QD above supported graphene.

where ω_L is the THz laser frequency of the pump field, σ^+/σ_- are the Pauli operators of the QD exciton, $\Omega = \langle \mathbf{E}_{\text{pump}}(\mathbf{r}_d) \rangle \cdot \mathbf{d}/\hbar$ is the effective Rabi frequency of the pump source (\mathbf{d} and \mathbf{r}_d are the QD dipole moment and position), \mathbf{f}^\dagger and \mathbf{f} are bosonic field operators, ω_x is the exciton resonance, and $\mathbf{E}(\mathbf{r}_d, \omega)$ is the total electric field operator at the QD position [17],

$$\mathbf{E}(\mathbf{r}, \omega) = i \sqrt{\frac{\hbar}{\pi \epsilon_0}} \int \sqrt{\text{Im}[\epsilon(\mathbf{r}', \omega)]} \mathbf{G}(\mathbf{r}, \mathbf{r}', \omega) \cdot \mathbf{f}(\mathbf{r}', \omega) d\mathbf{r}', \quad (2)$$

where the permittivity ϵ and Green function \mathbf{G} describe the photonic environment (reservoir) of the graphene and dielectric background. The Green tensor in the quantum field operator is the classical Green function (propagator) that provides the electromagnetic response at \mathbf{r} due to an excitation at \mathbf{r}' . All material parameters may be complex valued.

This Hamiltonian is used to form a quantum master equation as described in Ref. [11]. However, since we are interested in THz operation, we do not make the usual zero-temperature bath approximation. Using the traces $\text{Tr}_R[\mathbf{f}(\mathbf{r}, \omega) \mathbf{f}^\dagger(\mathbf{r}', \omega') \rho_R] = [\bar{n}(\omega) + 1] \delta(\mathbf{r} - \mathbf{r}') \delta(\omega - \omega')$ and $\text{Tr}_R[\mathbf{f}^\dagger(\mathbf{r}, \omega) \mathbf{f}(\mathbf{r}', \omega') \rho_R] = \bar{n}(\omega) \delta(\mathbf{r} - \mathbf{r}') \delta(\omega - \omega')$, where the average thermal photon number is $\bar{n} = (e^{\hbar\omega/k_B T} - 1)^{-1}$ and $\rho_R = \rho_R(0)$ is the density operator of the reservoir, which is assumed to initially be in thermal equilibrium, we obtain the master equation for the time evolution of the density operator [$\rho = \rho(t)$],

$$\begin{aligned} \frac{d}{dt} \rho = & -\frac{i}{\hbar} [H_S, \rho] - \int_0^t d\tau \{ J_{\text{ph}}^{\bar{n}+1}(\tau) [\sigma_+ \sigma_- (-\tau) \rho \\ & - \sigma_- (-\tau) \rho \sigma_+] + \text{H.c.} \} + L_{\text{pure}} - \int_0^t d\tau \{ J_{\text{ph}}^{\bar{n}}(-\tau) \\ & \times [\sigma_- \sigma_+ (-\tau) \rho - \sigma_+ (-\tau) \rho \sigma_-] + \text{H.c.} \}, \quad (3) \end{aligned}$$

where L_{pure} is a pure dephasing term defined in [11], $\sigma_\pm(-\tau) = e^{-iH_S\tau/\hbar} \hat{\sigma}_\pm e^{iH_S\tau/\hbar}$, $\tilde{J}_{\text{ph}}^{\bar{n}}(\tau) = \int_0^\infty d\omega J_{\text{ph}}(\omega) \bar{n}(\omega) e^{-i(\omega - \omega_L)\tau}$, and the photon reservoir function is related to the Green

function through

$$J_{\text{ph}}(\omega) = \frac{\mathbf{d} \cdot \text{Im}[\mathbf{G}(\mathbf{r}, \mathbf{r}, \omega)] \cdot \mathbf{d}}{\pi \hbar \epsilon_0}, \quad (4)$$

which gives a measure of the QD-environment coupling. Importantly, although at room temperature the average number of phonons at visible frequencies is negligible, in the low THz range $\bar{n} = O(1)$, so thermal photon effects are required in general.

We assume laterally infinite graphene modeled as an infinitesimally thin, local, two-sided surface characterized by a surface conductivity σ . The Green functions for a graphene sheet at the interface between two dielectrics are given in [5], and they are given in [12] for graphene on a finite-thickness dielectric support. Considering the graphene sheet in the plane $y = 0$, with material described by ϵ_1 for $y > 0$ and ϵ_2 for $y < 0$, the Green tensor for points in region n is

$$\underline{\mathbf{G}}(\mathbf{r}, \mathbf{r}') = (\mathbf{I} k_n^2 + \nabla \nabla \cdot) \{ \underline{\mathbf{g}}^p(\mathbf{r}, \mathbf{r}') + \underline{\mathbf{g}}^s(\mathbf{r}, \mathbf{r}') \}, \quad (5)$$

where $k_n = \omega \sqrt{\mu_0 \epsilon_n}$ is the wave number.

The principle (p) and scattered (s) Green function components are

$$\begin{aligned} \underline{\mathbf{g}}^p(\mathbf{r}, \mathbf{r}') &= \mathbf{I} \frac{e^{ik_n R}}{4\pi R}, \\ \underline{\mathbf{g}}^s(\mathbf{r}, \mathbf{r}') &= \widehat{\mathbf{y}} \widehat{\mathbf{y}} g_n^s(\mathbf{r}, \mathbf{r}') + \left(\widehat{\mathbf{y}} \widehat{\mathbf{x}} \frac{\partial}{\partial x} + \widehat{\mathbf{y}} \widehat{\mathbf{z}} \frac{\partial}{\partial z} \right) g_c^s(\mathbf{r}, \mathbf{r}') \\ &\quad + (\widehat{\mathbf{x}} \widehat{\mathbf{x}} + \widehat{\mathbf{z}} \widehat{\mathbf{z}}) g_t^s(\mathbf{r}, \mathbf{r}'), \quad (6) \end{aligned}$$

where \mathbf{I} is the unit dyadic, k_ρ is a radial wave number, $p_n^2 = k_\rho^2 - k_n^2$, $r = \sqrt{(x - x')^2 + (z - z')^2}$, and $R = |\mathbf{r} - \mathbf{r}'| = \sqrt{(y - y')^2 + r^2}$. The Sommerfeld integrals are

$$g_\beta^s(\mathbf{r}, \mathbf{r}') = \frac{1}{2\pi} \int_{-\infty}^{\infty} C_\beta \frac{H_0^{(1)}(k_\rho r) e^{-p(y+y')}}{4p} k_\rho dk_\rho, \quad (7)$$

where $\beta = t, n, c$ depends on the graphene and dielectric support layers. For a pump polarized perpendicular to the graphene surface we only need G_{zz} and $\beta = n$, with

$$C_n = \frac{\left(\frac{\epsilon_2}{\epsilon_1} p_1 - p_2 \right) i \omega \epsilon_1 - \sigma p_1 p_2}{\left(\frac{\epsilon_2}{\epsilon_1} p_1 + p_2 \right) i \omega \epsilon_1 - \sigma p_1 p_2}. \quad (8)$$

For more complex geometries, such as graphene on a multi-layered dielectric, only the coefficient C_n changes.

The wave parameter $p_n = \sqrt{k_\rho^2 - k_n^2}$ leads to branch points at $k_\rho = \pm k_n$, and thus the k_ρ plane is a four-sheeted Riemann surface. The standard hyperbolic branch cuts [18] that separate the proper sheet [where $\text{Re}(p_n) > 0$, such that the radiation condition as $|y| \rightarrow \infty$ is satisfied] and the improper sheet are the same as in the absence of surface conductivity σ . The zeros of the denominators of C_β lead to pole singularities in the spectral plane associated with SPPs. Using complex-plane analysis, the scattered Green function can be written as discrete pole (SPP) contributions plus a branch-cut integral over the continuum of radiation modes. For $\epsilon_1 = \epsilon_2 = \epsilon$, setting the denominator of (8) to zero leads to the (TM) SPP wave number $k_\rho = k \sqrt{1 - \left(\frac{2}{\sigma \eta} \right)^2}$, where $\eta = \sqrt{\mu_0/\epsilon}$. In this case, the vertical wave-number parameter in the Sommerfeld

integrals becomes $p = \sqrt{k_\rho^2 - k^2} = i2\omega\epsilon/\sigma$, and if σ is real-valued, then $\text{Re}(p) > 0$ is violated, and the TM mode is on the improper Riemann sheet. Assuming complex-valued conductivity $\sigma = \sigma' + i\sigma''$, $p = \frac{i2\omega\epsilon}{\sigma} = \frac{2\omega\epsilon}{|\sigma|^2}(\sigma'' + i\sigma')$, and therefore, if $\sigma'' > 0$ (as shown below, when the intraband conductivity dominates), the mode is a surface wave on the proper sheet, whereas if $\sigma'' < 0$ (interband conductivity dominates), the mode is on the improper sheet, assuming an $\exp(-i\omega t)$ reference [4,5]. Assuming the dipole moment is perpendicular to the graphene surface, only TM SPPs can be excited.

The graphene surface conductivity is [19]

$$\sigma(\omega) = \frac{ie^2k_B T}{\pi\hbar^2(\omega + i\gamma)} \left[\frac{\mu_c}{k_B T} + 2 \ln\left(e^{-\frac{\mu_c}{k_B T}} + 1\right) \right] + \frac{ie^2(\omega + i\Gamma)}{\pi\hbar^2} \int_0^\infty \frac{f_d(-\epsilon) - f_d(\epsilon)}{(\omega + i\Gamma)^2 - 4(\epsilon/\hbar)^2} d\epsilon, \quad (9)$$

where μ_c is the chemical potential, γ and Γ are phenomenological intraband and interband scattering rates, respectively ($\tau = 1/\gamma$ is the scattering time), e is the charge of an electron, and $f_d(\epsilon) = (e^{\epsilon - \mu_c}/k_B T + 1)^{-1}$ is the Fermi-Dirac distribution. The first and second terms in the conductivity are due to intraband and interband contributions, respectively. For $k_B T \ll |\mu_c|, \hbar\omega$ [20],

$$\sigma(\omega) = \frac{ie^2|\mu_c|}{\pi\hbar(\omega + i\gamma)} + \frac{ie^2}{4\pi\hbar} \ln\left(\frac{2|\mu_c| - (\omega + i\Gamma)\hbar}{2|\mu_c| + (\omega + i\Gamma)\hbar}\right). \quad (10)$$

In the following we use (9) for $T = 300$ K and (10) for $T = 0$ K calculations. We consider a local (momentum independent) conductivity since the main effect considered here is the nontrivial DOS provided by the graphene plasmon energy dispersion. The Drude form of the conductivity has been verified in the far infrared [21–27], and in the near infrared and visible the interband behavior has been verified in [25]. In the absence of scattering and bias the high-frequency optical conductivity is $\sigma = \sigma_{\min} = e^2/4\hbar$, which has been verified in optical experiments [28].

Absorption is associated with both scattering and interband transitions. Since realistic values of Γ will have a negligible effect on the results, we will ignore interband scattering. For $\hbar\omega < 2|\mu_c|$, interband absorption is blocked; otherwise, interband absorption will often dominate $\text{Re}(\sigma)$. For the intraband term the value of γ generally depends on temperature via phonon interactions, the method of growth/fabrication (e.g., epitaxy, chemical vapor deposition, exfoliation), the presence of impurities, and the presence of a substrate. Measured values of scattering times at room temperature ranged from a few femtoseconds [21,22] to several tens of femtoseconds [21–23] to several hundred femtoseconds (~ 0.35 ps [26,27]), and at low temperature scattering times on the order of a few picoseconds have been measured (1.1 ps [25] and 5 ps [23]). Short scattering times are usually associated with impurities and defects since the room-temperature electron-phonon scattering time is estimated to be a few picoseconds [24]. In the following we assume $\tau = 5$ ps for $T = 0$ and $\tau = 0.35$ ps for room-temperature results. We assume lossless nondispersive

dielectrics to focus on graphene's electrodynamic response rather than on the substrate response.

III. PURCELL FACTORS

The partial LDOS projected normal to the graphene surface, $\rho_{\text{LDOS}} = (6/\pi\omega)\text{Im}[G_{zz}(\mathbf{r}, \mathbf{r}, \omega)]$, normalized by the free-space value $\rho_{\text{LDOS}}^0 = \omega^2/(\pi^2 c^3)$ gives the Purcell factor [1] (i.e., the enhanced spontaneous emission factor of a single-photon emitter),

$$\text{PF} = \frac{\rho_{\text{LDOS}}}{\rho_{\text{LDOS}}^0} = \frac{6\pi}{k_0^3} \text{Im}[G_{zz}(\mathbf{r}, \mathbf{r}, \omega)]. \quad (11)$$

In the following we consider both suspended graphene, where vacuum exists on either side of the graphene sheet, and supported graphene on a dielectric layer. Figure 2(a) shows the tunability of the Purcell factor [29] at THz frequencies for a single suspended graphene layer over a range of chemical potentials at a distance of 10 nm from the graphene surface for $\mu_c/k_B T \gg 1$ and $\omega/\gamma \gg 1$ (at room temperature the results of Fig. 2 will hold with minor quantitative changes). It is clear that in the low-THz regime the LDOS and Purcell factor can be tuned considerably by an external bias. Figure 2(b) shows the Purcell factor for supported graphene on a $d_s = 10$ nm thin substrate having relative permittivity $\epsilon_r = 4$ (the approximate permittivity of SiO_2). The presence of the substrate perturbs the SPP of the suspended graphene sheet and clearly redshifts the Purcell factor maximums (larger values of ϵ_r would further redshift the Purcell factor). As discussed in [12], the presence of a substrate tends to confine the SPP mode, leading to higher attenuation as energy concentrates at the lossy graphene surface. Figure 2(c) shows the Purcell factor (PF) for two layers of graphene separated by a 10-nm, $\epsilon_r = 4$ substrate. This case closely resembles the result of Fig. 2(b), although the bottom graphene layer leads to a parallel-plate-like waveguide structure [30], which tends to further concentrate energy in the dielectric, narrowing and shifting the PF peaks. Figure 2(d) shows the Purcell factor as a function of position

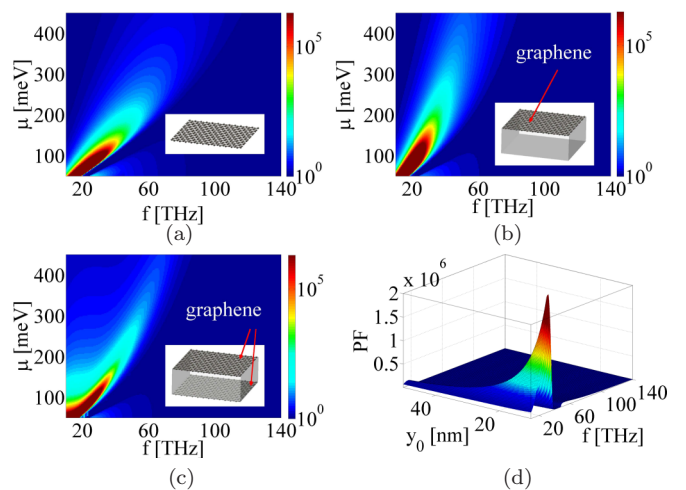


FIG. 2. (Color online) The Purcell factor (a) for suspended graphene in vacuum, (b) for graphene on a $d_s = 10$ nm, $\epsilon_r = 4$ substrate, (c) for two layers of graphene separated by a 10-nm, $\epsilon_r = 4$ substrate, and (d) as a function of position (y_0 is the dot position) and frequency for supported graphene on a 10-nm, $\epsilon_r = 4$ substrate.

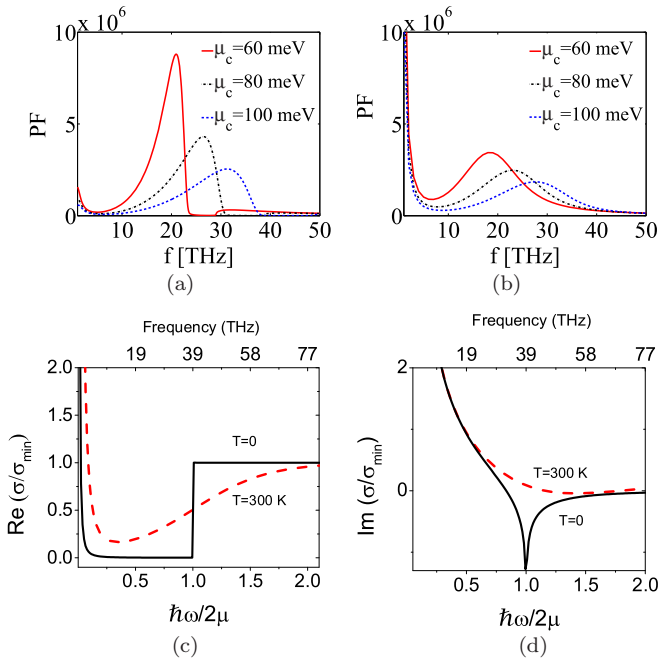


FIG. 3. (Color online) Purcell factor for suspended graphene for three different chemical potentials at (a) $T = 0$ K and (b) $T = 300$ K. (c) Real and (d) imaginary parts of graphene conductivity at $\mu_c = 80$ meV normalized by $\sigma_{\min} = e^2/4\hbar = 6.085 \times 10^{-5}$ S.

and frequency for supported graphene on a 10-nm, $\epsilon_r = 4$ substrate. Clearly, to be able to tune the QD resonance fluorescence, the QD needs to be located sufficiently close to the graphene surface to strongly couple to the graphene SPP due to the strong confinement of the SPP mode. However, one of the advantages of using graphene sheets is that this coupling is translationally invariant in the x and z directions.

Figure 3 shows the Purcell factor for suspended graphene for three different values of chemical potential at $T = 0$ [Fig. 3(a)] and $T = 300$ K [Fig. 3(b)]. It can be seen that at the higher temperature the peaks are broadened due to higher absorption compared to the $T = 0$ result. Figures 3(c) and 3(d) show the conductivity for the $\mu_c = 80$ meV case. As frequency increases from a low value, the Drude (intraband) term drops off at γ , and the interband contribution becomes more important, with a sharp transition in the real part when $\alpha = \hbar\omega/2\mu_c = 1$. The imaginary part undergoes a cusp discontinuity (for $T = 0$ K) at $\alpha = 1$. When $\text{Im}(\sigma) < 0$, which occurs in the vicinity of the cusp, the TM SPP cannot propagate (generally, when this occurs, a TE SPP can propagate, although for a vertical dipole excitation the TE SPP will not be excited), and this is associated with the drop-off of the Purcell factor. The peak in the Purcell factor corresponds approximately to the frequency where $\text{Im}(\sigma) = \text{Re}(\sigma)$.

IV. SPECTRUM OF A DRIVEN QUANTUM DOT

The incoherent spectrum is defined as

$$S_0(\omega) = \lim_{t \rightarrow 0} \text{Re} \int_0^\infty d\tau \langle \sigma_+(t+\tau) \sigma_-(t) \rangle - \langle \sigma_+(t) \rangle \langle \sigma_-(t) \rangle e^{i(\omega_L - \omega)\tau} d\tau, \quad (12)$$

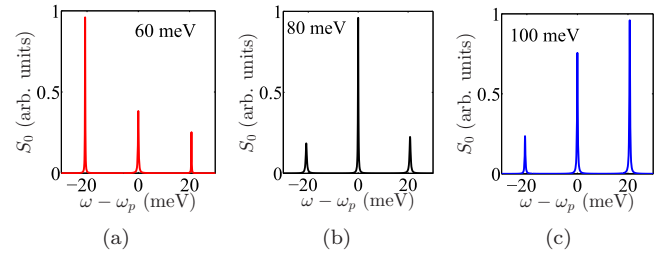


FIG. 4. (Color online) Incoherent spectrum of the QD 10 nm above graphene, pumped at 25 THz with (a) $\mu_c = 60$ meV, (b) $\mu_c = 80$ meV, and (c) $\mu_c = 100$ meV.

where the second term subtracts the coherent scattering from the pump field. The incoherent spectrum of the QD is shown in Figs. 4(a)–4(c) for a Rabi frequency of 10 meV at 25 THz, assuming $T = 0$ [see the Purcell factor in Fig. 3(a)]; in all subsequent results the dipole moment is taken to be 30 D. Note that the pump field will naturally be efficiently increased by the coupling to the SPP. It is evident that by changing the chemical potential of graphene the weights of the Mollow triplet sidebands can be substantially changed. That is, the dominant peak of the incoherent spectrum can be shifted, for example, by varying the bias voltage on graphene. As Fig. 3 shows, by varying the bias we can shift the peak of the LDOS; when the LDOS peak aligns with the peak of one of the Mollow triplets, the corresponding triplet is enhanced. Commensurately, a small value of the LDOS at the position of a triplet peak suppresses that peak (due to closure of the plasmon decay channel). This is one of the key results of the paper: the quantum coupling between QDs and graphene can be profoundly influenced by simply changing the bias field.

Note that in all three cases in Fig. 4 the exciton-laser detuning is zero ($\omega_x = \omega_L$), and it is solely the change in the LDOS with bias that is responsible for the significant spectrum tuning. As seen in Fig. 3(b), at $T = 300$ K the peaks are broadened but are not significantly shifted compared to the $T = 0$ case. Therefore, at room temperature the Mollow triplet can also be controlled. However, in this case, since the peaks overlap more than for $T = 0$, it is advantageous to choose the Rabi frequency (which controls the separation of the triplet's peaks) and chemical potential values (which control the Purcell factor peaks) to further separate the peaks to achieve similar control over the triplet as in the low-temperature case.

The far-field detectable spectrum at position \mathbf{r}_D is defined as [11] $S_p(\mathbf{r}_D, \omega) = \frac{2}{\epsilon_0} |\mathbf{d} \cdot \mathbf{G}(\mathbf{r}_D, \mathbf{r}_d, \omega)|^2 S_0(\omega)$. The factor that multiplies S_0 has some features in the vicinity of $\mathbf{r}_D = \lambda_{\text{SPP}}$ but is otherwise dominated by the homogeneous-space part of the Green function and is fairly featureless, so the Mollow triplet of the detectable spectrum will resemble S_0 .

In Fig. 3 the considered values of μ_c lead to peaks of the Purcell factor in the range 20–30 THz. For these bias values and frequencies interband absorption is blocked, and the only damping of the conductivity is due to scattering. At several tens of THz and room temperature, $\mu_c/k_B T \gg 1$ is at least weakly satisfied, and the Purcell factor results do not change qualitatively from the $T = 0$ K results, although enhanced absorption broadens the curves [Fig. 3(b)]. Furthermore, at several tens of THz, even at room temperature, the average photon number \bar{n}

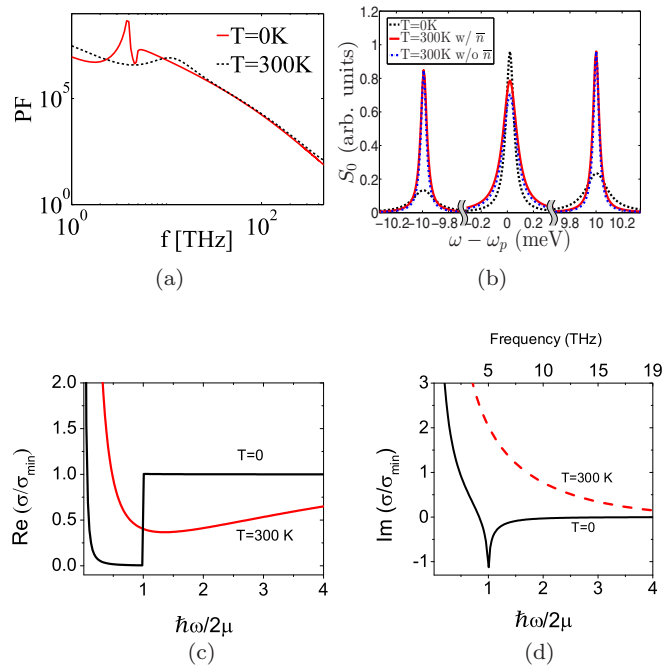


FIG. 5. (Color online) (a) Purcell factor for suspended graphene at $x = 10$ nm and $\mu_c = 10$ meV at $T = 0$ K and $T = 300$ K. (b) The incoherent spectrum of the QD above graphene for a Rabi frequency of 10 meV and pump resonance at 4 THz, with and without including \bar{n} ; (c) and (d) show the corresponding conductivity.

is negligible, and so the zero-temperature bath approximation holds. However, for small enough bias the Purcell factor peaks below a few THz, in which case both $\mu_c/k_B T \gg 1$ and $\omega/\gamma \gg 1$ are violated at room temperature. At frequencies of a few THz and for small bias, temperature plays an important role both in the Purcell factor via the graphene conductivity (interband transitions will not be blocked, leading to enhanced absorption, and the location of the PF peak blueshifts due to the second inequality being violated)

and in the incoherent spectrum via the effect of the average photon number being non-negligible. To examine this effect, Fig. 5(a) shows the Purcell factor at $x = 10$ nm and $\mu_c = 10$ meV at $T = 0$ K and $T = 300$ K. Figure 5(b) shows the effect on the resonance fluorescence spectrum. Also shown is the effect of including \bar{n} in the $T = 300$ K calculation, where it can be seen that the inclusion of the room-temperature thermal bath is important at these low THz frequencies. Figures 4(c) and 4(d) show the normalized conductivity; compared to the 300 K result in Figs. 3(c) and 3(d) for $\mu_c = 80$ meV, here the intraband contribution is still important when the interband term becomes active, significantly perturbing the LDOS from the $T = 0$ K case (the Drude falloff is set by τ , and the onset of interband absorption is set by μ_c , so these two effects can be independently controlled, although μ_c also governs the amplitude of the intraband contribution). Since we keep the same pump frequency for $T = 0$ K and $T = 300$ K, in the latter case the LDOS is relatively flat at the pump frequency.

V. CONCLUSIONS

In conclusion, we have shown that the Purcell effect and the Mollow triplet of a two-level emitter can be tuned by varying the chemical potential of a nearby graphene layer. We have modeled this effect using an exact Green function theory for the LDOS and exploited a quantum master equation to model the quantum dynamics. We have also demonstrated the important influence of temperature. This novel QD-graphene system allows considerable spectral control at the quantum level via altering easily assessable external parameters of the system.

ACKNOWLEDGMENTS

This work was supported by the Natural Sciences and Engineering Research Council of Canada. We thank R. Ge for useful discussions.

- [1] E. M. Purcell, *Phys. Rev.* **69**, 37 (1946).
- [2] B. Wunsch, T. Stauber, F. Sols, and F. Guinea, *N. J. Phys.* **8**, 318 (2006).
- [3] E. H. Hwang and S. Das Sarma, *Phys. Rev. B* **75**, 205418 (2007).
- [4] S. A. Mikhailov and K. Ziegler, *Phys. Rev. Lett.* **99**, 016803 (2007).
- [5] G. W. Hanson, *J. Appl. Phys.* **103**, 064302 (2008).
- [6] J. Chen, M. Badioli, P. Alonso-González, S. Thongrattanasiri, F. Huth, J. Osmond, M. Spasenović, A. Centeno, A. Pesquera, P. Godignon, A. Z. Elorza, N. Camara, F. J. G. de Abajo, R. Hillenbrand, and F. H. L. Koppens, *Nature (London)* **487**, 77 (2012).
- [7] H. Yan, T. Low, W. Zhu, Y. Wu, M. Freitag, X. Li, F. Guinea, P. Avouris, and F. Xia, *Nat. Photonics* **7**, 394 (2013).
- [8] F. H. L. Koppens, D. E. Chang, and F. J. Garcia de Abajo, *Nano Lett.* **11**, 3370 (2011).
- [9] A. Manjavacas, S. Thongrattanasiri, D. E. Chang, and F. J. Garcia de Abajo, *New J. Phys.* **14**, 123020 (2012).
- [10] H. J. Carmichael, *Statistical Methods in Quantum Optics I* (Springer, Berlin, 2002).
- [11] R.-C. Ge, C. V. Vlack, P. Yao, J. F. Young, and S. Hughes, *Phys. Rev. B* **87**, 205425 (2013).
- [12] G. W. Hanson, E. Forati, W. Linz, and A. B. Yakovlev, *Phys. Rev. B* **86**, 235440 (2012).
- [13] E. A. Zibik, T. Grange, B. A. Carpenter, N. E. Porter, R. Ferreira, G. Bastard, D. Stehr, S. Winnerl, M. Helm, H. Y. Liu, M. S. Skolnick, and L. R. Wilson, *Nat. Mater.* **8**, 803 (2009).
- [14] H. Hashiba, V. Antonov, L. Kulik, A. Tzalenchuk, P. Kleinschmid, S. Giblin, and S. Komiyama, *Phys. Rev. B* **73**, 081310(R) (2006).
- [15] B. R. Mollow, *Phys. Rev.* **188**, 1969 (1969).
- [16] R. Loudon, *The Quantum Theory of Light*, 3rd ed., Oxford Science Publications (Oxford University Press, Oxford, 2000).
- [17] T. Gruner and D. G. Welsch, *Phys. Rev. A* **53**, 1818 (1996).
- [18] A. Ishimaru, *Electromagnetic Wave Propagation, Radiation, and Scattering* (Prentice Hall, Englewood Cliffs, NJ, 1991).

- [19] V. P. Gusynin, S. G. Sharapov, and J. P. Carbotte, *J. Phys. Condens. Matter* **19**, 026222 (2007).
- [20] V. P. Gusynin, S. G. Sharapov, and J. P. Carbotte, *Phys. Rev. B* **75**, 165407 (2007).
- [21] J. M. Dawlaty, S. Shivaraman, J. Strait, P. George, Mvs Chandrashekhar, F. Rana, M. G. Spencer, D. Veksler, and Y. Chen, *Appl. Phys. Lett.* **93**, 131905 (2008).
- [22] H. Choi, F. Borondics, D. A. Siegel, S. Y. Zhou, M. C. Martin, A. Lanzara, and R. A. Kaindl, *Appl. Phys. Lett.* **94**, 172102 (2009).
- [23] Y.-W. Tan, Y. Zhang, K. Bolotin, Y. Zhao, S. Adam, E. H. Hwang, S. Das Sarma, H. L. Stormer, and P. Kim, *Phys. Rev. Lett.* **99**, 246803 (2007).
- [24] C. Berger, Z. Song, X. Li, X. Wu, N. Brown, C. Naud, D. Mayou, T. Li, J. Hass, A. N. Marchenkov, E. H. Conrad, P. N. First, and W. A. de Heer, *Science* **312**, 1191 (2006). The 4-ps value is for electron-phonon scattering.
- [25] Z. Q. Li, E. A. Henriksen, Z. Jiang, Z. Hao, M. C. Martin, P. Kim, H. L. Stormer, and D. N. Basov, *Nat. Phys.* **4**, 532 (2008).
- [26] C. Lee, J. Y. Kim, S. Bae, K. S. Kim, B. H. Hong, and E. J. Choi, *Appl. Phys. Lett.* **98**, 071905 (2011).
- [27] J. Y. Kim, C. Lee, S. Bae, K. S. Kim, B. H. Hong, and E. J. Choi, *Appl. Phys. Lett.* **98**, 201907 (2011).
- [28] R. R. Nair, P. Blake, A. N. Grigorenko, K. S. Novoselov, T. J. Booth, T. Stauber, N. M. R. Peres, and A. K. Geim, *Science* **320**, 1308 (2008).
- [29] P. A. Huidobro, A. Y. Nikitin, C. González-Ballester, L. Martín-Moreno, and F. J. García-Vidal, *Phys. Rev. B* **85**, 155438 (2012).
- [30] G. W. Hanson, *J. Appl. Phys.* **104**, 084314 (2008).